



BNL-222854-2022-JAAM

Interferometric Bunch Length Measurements of 3 MeV Picocoulomb Electron Beams

X. Yang

To be published in "Journal of Applied Physics"

February 2022

Photon Sciences

Brookhaven National Laboratory

U.S. Department of Energy

USDOE Office of Science (SC), Basic Energy Sciences (BES) (SC-22)

Notice: This manuscript has been authored by employees of Brookhaven Science Associates, LLC under Contract No. DE-SC0012704 with the U.S. Department of Energy. The publisher by accepting the manuscript for publication acknowledges that the United States Government retains a non-exclusive, paid-up, irrevocable, world-wide license to publish or reproduce the published form of this manuscript, or allow others to do so, for United States Government purposes.

DISCLAIMER

This report was prepared as an account of work sponsored by an agency of the United States Government. Neither the United States Government nor any agency thereof, nor any of their employees, nor any of their contractors, subcontractors, or their employees, makes any warranty, express or implied, or assumes any legal liability or responsibility for the accuracy, completeness, or any third party's use or the results of such use of any information, apparatus, product, or process disclosed, or represents that its use would not infringe privately owned rights. Reference herein to any specific commercial product, process, or service by trade name, trademark, manufacturer, or otherwise, does not necessarily constitute or imply its endorsement, recommendation, or favoring by the United States Government or any agency thereof or its contractors or subcontractors. The views and opinions of authors expressed herein do not necessarily state or reflect those of the United States Government or any agency thereof.

Interferometric Bunch Length Measurements of 3 MeV Picocoulomb Electron Beams

X. Yang^{1*}, L. H. Yu¹, V. Smaluk¹, T. Shaftan¹, L. Doom¹, B. Kosciuk¹, W. X. Cheng², B. Bacha¹, D. Padrazo¹, J. J. Li¹, M. Babzien¹, M. Fedurin¹, G. L. Carr¹, Y. M. Zhu¹

¹Brookhaven National Laboratory, Upton, NY 11973, USA

²Advanced Photon Source, Argonne National Laboratory, Lemont, IL 60439, USA

ABSTRACT

We report picosecond bunch length measurements, using an interferometric method, for a 3 MeV electron beam having bunch charge ranging from 1 to 14 pC. The method senses the single-cycle sub-terahertz (THz) pulse emitted by each electron bunch as coherent transition radiation, which in turn is analyzed using Michelson-type interferometer, forming an interferogram that is then processed to yield the nominal electron bunch length. This sub-THz coherent radiation intensity was measured using a quasi-optical detector (QOD) operating at room temperature. This experiment was quite challenging since the divergence angle of the sub-THz pulse emitted by the low-energy electron bunch exceeds $\pm 10^\circ$, and its pulse energy at the entrance to the detector was as low as a 100 picojoules. When compared to a conventional helium-cooled silicon composite bolometer designed for frequencies above 0.5 THz, the QOD provided much better signal-to-noise ratio in the ~ 80 GHz frequency range, which was critical for the successful measurement of the bunch length.

I. INTRODUCTION

Mega-electron-volt ultrafast-electron-diffraction (MeV-UED) takes advantage of the strong Coulomb interaction between electrons and the distribution of charges in matter, as well as mitigation of some space charge effects¹⁻⁶. Compared to 10 keV X-rays, which are typically produced in synchrotron light sources, 3 MeV electrons have a 350-fold shorter wavelength and thus can resolve much finer structural details. When the probing electrons are packed in a very short bunch, single-shot MeV-UED enables one to determine the instantaneous positions of atoms, and multiple shots with various delays can be used to follow atomic motion, making molecular movies of ultrafast chemical reactions^{7,8}. This has led to increasing interest in the development of single-shot MeV-UED facilities. At Brookhaven National Laboratory (BNL), we demonstrated that one can focus the transverse size of a 3 MeV 14 pC electron beam down to 40 μm using a broadly tunable electromagnetic quadrupole lens system⁹. This focusing system significantly improves the MeV-UED instrument, and it is a step closer to achieving the electron beam quality

required for single-shot UED by providing the brightness several orders of magnitude higher than current technology¹⁰⁻¹⁴.

Single-shot UED requires an electron beam with a high charge and high brightness simultaneously. Characterizing the brightness of an electron beam in 6D phase space requires measurements of the transverse beam size and divergence, as well as the bunch length and energy spread^{15,16,17}. The bunch length measurement becomes critically important for understanding the intensity-dependent bunch lengthening caused by space charge effects. Benchmarking the measured data with numerical simulations via the General Particle Tracer (GPT) code¹⁸ can help us in developing a virtual diagnostic tool for online monitoring the electron bunch profile. Together with the Bragg-diffraction method measuring the electron beam divergence, energy, and energy spread, the interferometric measurement of the bunch length will complete the 6D phase space diagnostics.

II. MEASUREMENT TECHNIQUE

Several prior techniques have been developed to measure the bunch length of low-energy and low-charge electron beams. Some methods use the laser-driven THz streaking technique to sample very short timescales ($<10^{-13}$ s), and ultrafast-laser-pump with electron-beam-probing on 10^{-14} s to 10^{-12} s timescale were reported^{10,19-22}. The bunch length could be estimated by deconvolving all other factors from the measurement results. Compared to this pump-probe method, the advantages of measuring the bunch length of a 3 MeV electron beam using an interferometer are:

- The experimental setup is greatly simplified because there is no need for arranging both laser and electron beam to meet and overlap at a sample location.
- The timing jitter between the laser and electron beams does not contribute any error to the bunch length measurement.
- The method can be easily extended to a sub-picosecond regime, enabling bunch length measurement in a much broader timescale from 10^{-14} s to 10^{-11} s.

As the radiated pulse energy reaching the detector can be as low as 100 picojoules, applying the interferometric technique to low-energy (3 MeV) and low-charge (a few pC) electron beams requires a detector with good signal-to-noise ratio (SNR) for the relevant spectral range.

At the BNL UED facility, we successfully measured the bunch length of a 3 MeV picocoulomb electron beam using a far-infrared Michelson interferometer and a Schottky-based QOD²³. The QOD model ‘3DL-12C-2500LS-A2’ from ACST has the proper frequency bandwidth from 30 GHz to 1.0 THz (with peak response near 70 GHz). Based on $\Delta t \approx 1/2\pi f$, this detector should be nearly optimal for bunch lengths in the 2 ps range. We compared the QOD response to sub-THz coherent transition radiation with that of a far-infrared spectroscopy bolometer operating at T=4.2K. This standard bolometer is optimized for the 0.6 to 18 THz spectral range and uses an f/3.5 Winston cone to control the field-of-view. The cone exit aperture is about 2 mm in diameter and acts as a high-pass filter starting near 400 GHz. As such, this type of detector works best for bunch lengths in the 40 fs or shorter regime. This is consistent with our experimental results where the QOD provided a SNR more than 20 times higher than this conventional spectroscopy bolometer in the sub-THz frequency range. The QOD has the additional benefit of room temperature operation as well as a compact package, plus, it is well-matched to the bunch lengths frequently encountered with low-energy electron beams.

In our experiment, the electron bunch was longer than 1 ps due to the effective lengthening of the drive laser pulse. The incident angle of the laser pulse to the photocathode is 70° (called oblique incidence), which causes different parts of the pulse-front to arrive at the photocathode at different times. This effect makes the electron bunch significantly longer than the laser pulse. This undesirable lengthening can be corrected by compensation optics, which, however, haven’t been implemented at the BNL Accelerator Test Facility II (ATF-II). Instead, we adjusted the electron bunch length by varying the laser spot size on the photocathode. We were able to vary the bunch length in the range of 1 to 5 ps, which will be described in detail later.

III. RESULTS AND DISCUSSION

3.1 Experimental Results

A schematic layout of the bunch length measurement carried out at the BNL UED facility is shown in Fig. 1. A bunched 3 MeV electron beam is generated by a radiofrequency photoinjector based on a copper photocathode illuminated with a short laser pulse at 265 nm wavelength as produced in a frequency-tripled Ti-sapphire laser system. The electron beam travels to an aluminum (Al) target where a single-cycle sub-nanojoule coherent THz pulse is produced as coherent transition radiation (CTR)²⁴. The charge of an electron beam can be varied from 1 to 14

pC by changing the drive laser pulse energy. An electron beam with a kinetic energy of 3 MeV has a Lorentz factor γ equal to 6.87. The far-field radiated intensity from a 3 MeV electron beam peaks near an angle $\theta = 1/\gamma$ just over 8° . This sub-THz pulse is extracted from the accelerator vacuum pipe through a 35-mm diameter window made of high-density polyethylene having $> 90\%$ transmission in this spectral frequency range²⁵. The diverging sub-THz radiation is collimated by a parabolic mirror having an effective focal length $f = 152$ mm to form an approximately collimated beam entering the far-infrared Michelson interferometer. The angular acceptance of the system is determined by the ratio of the window radius to the distance from the radiator to the window. In our case, the acceptance is 17.5° , which is about $2 \cdot 1/\gamma$. As a result, the system collects about 50% of the emitted sub-THz radiation. In the interferometer, the sub-THz pulse is split into two by a 50/50 beam splitter (BS), and one pulse is delayed by a variable interval τ with respect to the other. The two pulses are then recombined and detected by the QOD. Only half of the incident energy goes into the QOD, while the other half is lost in the retroreflected path back to the source. When the path-length difference exceeds the bunch length, the detected intensity is constant with delay τ , and this constant signal level is called the baseline. If the path-length difference is smaller than the bunch length, the intensity varies about the baseline. The detected intensity as a function of the delay τ is the interferogram. The width of the interferogram peak is used to estimate the bunch length²⁶⁻³⁰. For a Gaussian beam, the root mean square (RMS) bunch length σ_t is determined by
$$\frac{\text{interferogram FWHM}}{\sqrt{2\pi}}.$$

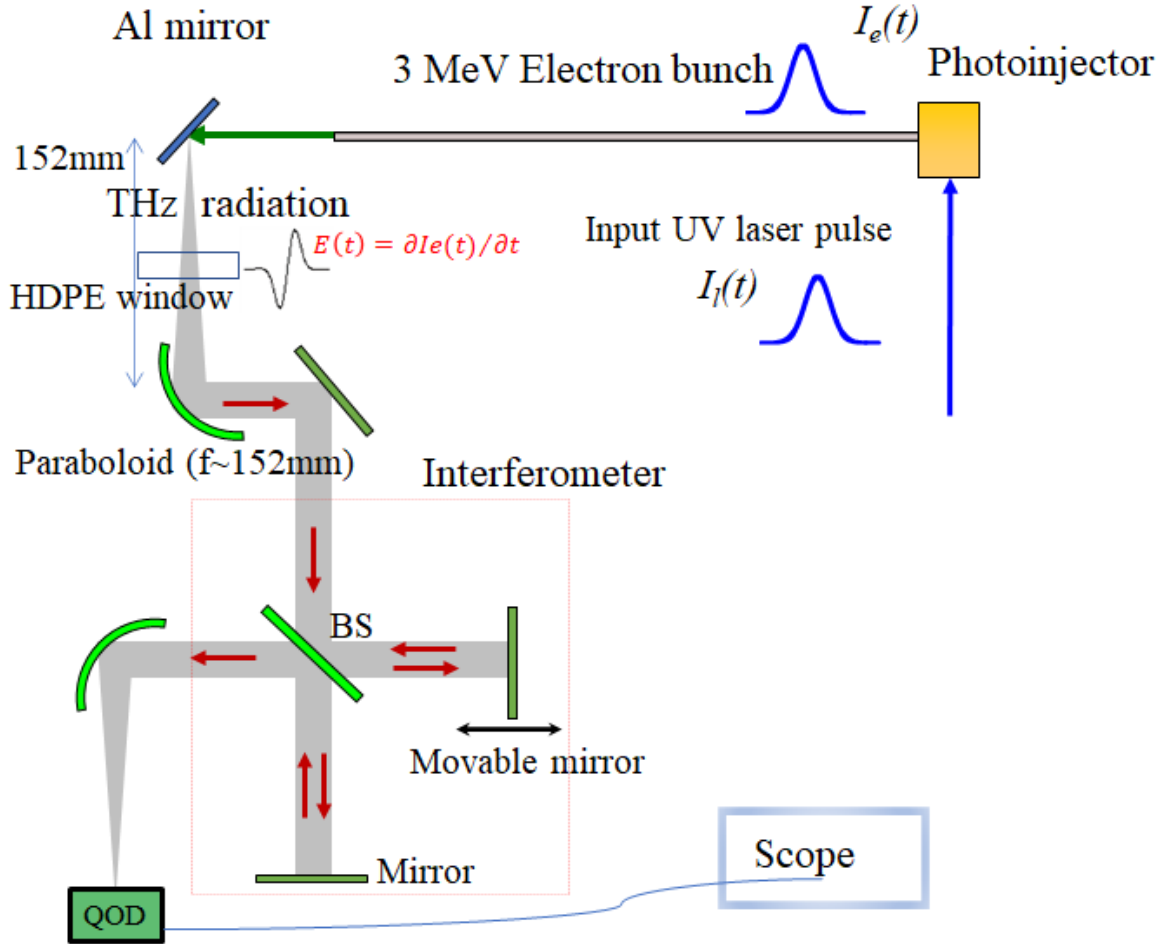


FIG. 1. Schematic of the bunch length measurement setup. HDPE represents high density polyethylene.

We numerically studied whether the QOD frequency response distorted the interferogram. In the experimental setup, either a QOD or a bolometer can be installed as the detector to measure the signal of the interferogram. The QOD frequency response provided by the manufacturer is shown as the reference (red curves) in the right graphs of Fig. 2. The left graphs of Fig. 2 show the interferograms calculated with two different values of RMS bunch length: 1.8 ps (top) and 4.5 ps (bottom). For a certain bunch length and the frequency response of a detector, the convolution of the bunch current profile and its replica with a variable time delay τ forms the interferogram. Assuming a Gaussian current profile, we multiply the Fourier transform of the interferogram by the detector frequency response and then apply the inverse Fourier transform to obtain the interferograms shown in Fig. 2. For every bunch length, the interferograms were calculated with two different conditions, the QOD frequency response (blue curves in the left graphs) and the flat response of a bolometer (red curves in the left column). The interferograms shown in Fig. 2

correspond to the lower and upper limits of the measured bunch length, so we can conclude the QOD frequency response does not affect the measurement results in our case.

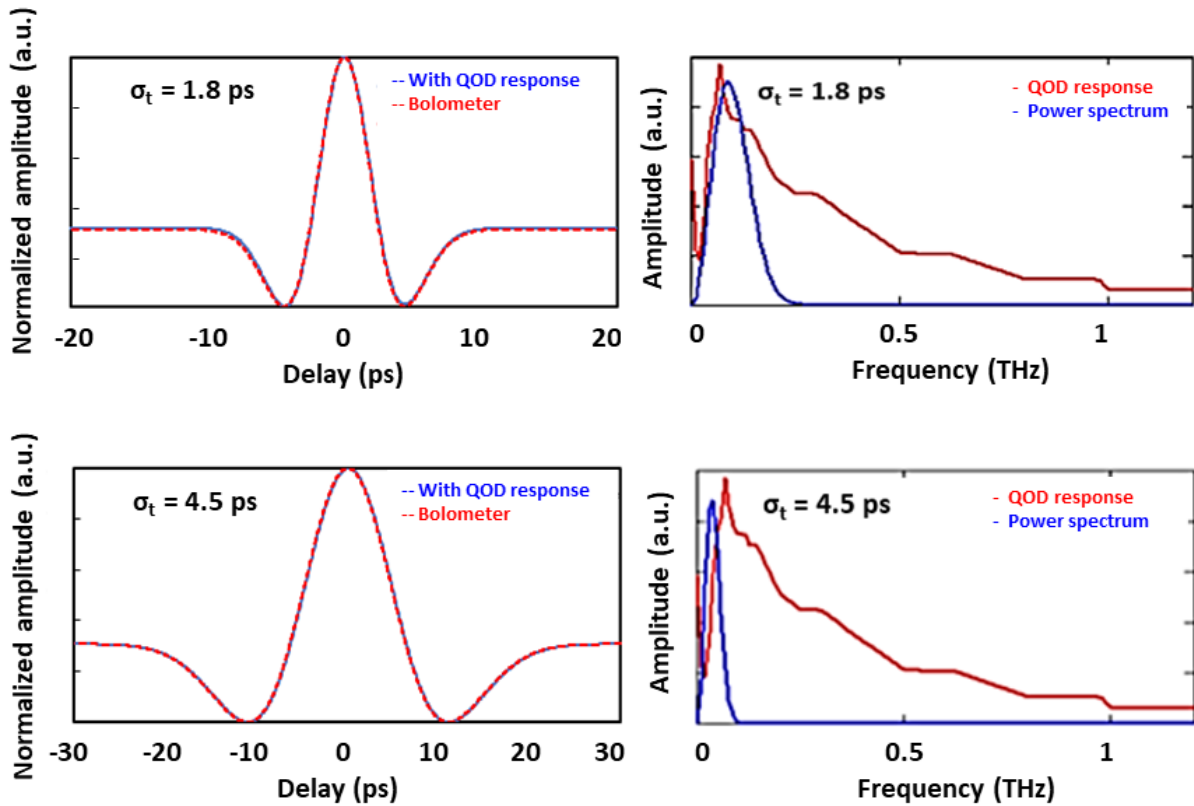


FIG. 2. Simulated interferograms (left graphs) and their Fourier spectra (blue curves in the right graphs) at two different bunch lengths in RMS: 1.8 ps (top graphs) and 4.5 ps (bottom graphs). For each bunch length, the interferograms with the QOD frequency response (blue) and with the flat response of a bolometer (red) are plotted. The QOD frequency response is plotted as the red curve in the right column as the reference.

We experimentally compared the signal-to-noise ratio of the bolometer and the QOD. The bolometer used is a commercial liquid-helium cooled composite silicon detector from INFRARED LABORATORIES³¹, operating at 4.2 K. For this type of detector, the noise typically comes from thermal fluctuations of the $T=295$ K environment. For the beam charge of 10 pC and bunch length of 4.0 ps, the peak signal measured by the bolometer was 25 mV (Fig. 3a) and the signal measured by the QOD was 500 mV (Fig. 3b). To take the detector response time into account, the sample rate of the oscilloscope (Keysight Infiniium 9040A) was set to 400 MHz for the bolometer and 20 GHz for the QOD. The noise level for both detectors was similar, about 5 mV (note different scales in Figs. 3a and 3b). We determined that the bolometer doesn't have an adequate SNR to measure the interferogram as the required SNR should be ≥ 6 (details in the Discussion section), therefore

a minimum signal of 30 mV (peak) is needed. Compared to a conventional bolometer, the significantly improved sensitivity of a QOD enables the interferometric measurement of the bunch length for a low energy (3 MeV) and low charge (1 pC) electron beam. The stepper motor moving the mirror with a sub- μm precision contributes an error of few femtoseconds, which is quite small considering the measured bunch lengths of a few picoseconds. Separately, the motor was repositioned to the reference position with a sub- μm precision, after each scan of the interferogram. The minimum step size for the movable mirror is 2 μm , which limits the resolution of the bunch length measurement to 13 fs. In the experiment, a step size of 10 μm was used, every step was confirmed by the position readback from the encoder. The oscilloscope was triggered after every step to record the QOD signal. The measurement time of one interferogram was about 20 minutes at a repetition rate of 5 Hz.

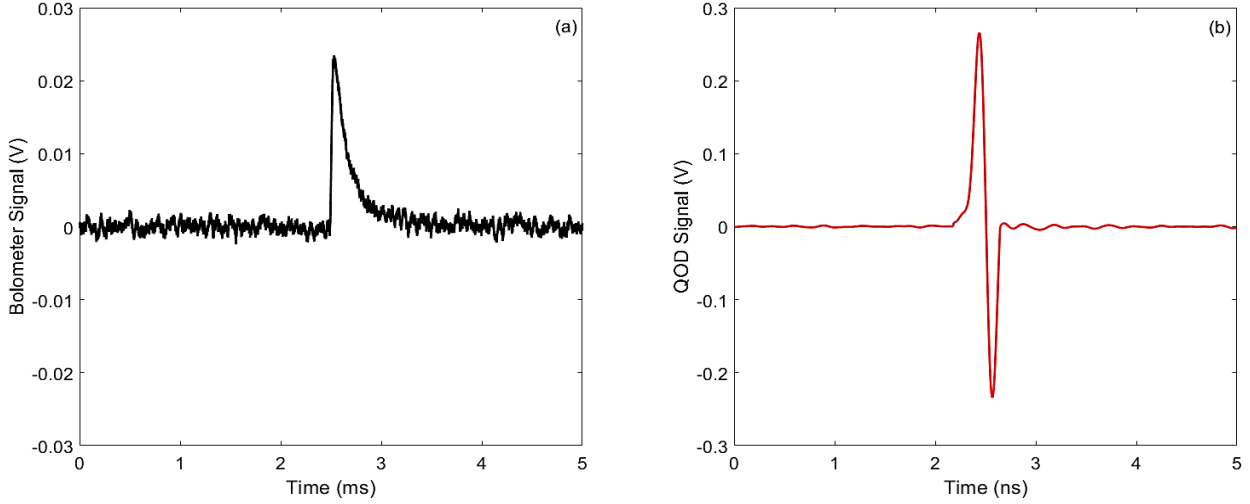


FIG. 3. (a) For the charge of 10 pC and bunch length 4.0 ps case, Bolometer signal is plotted as the black curve. (b) For the same case, the QOD signal is plotted as the red curve.

To take advantage of varying the electron bunch length via changing the laser size on the photocathode, we measured the bunch length at two different laser sizes Σ_x in full-width half maximum (FWHM): 707 μm and 289 μm . The effective FWHM laser pulse length is

$$\Sigma_{t,laser} = \Sigma_x \times \sin \theta / c. \quad (1)$$

Here, $\theta = 70^\circ$ is the incident angle of the laser pulse to the photocathode and c is the speed of light. The laser spot sizes of 707 μm and 289 μm correspond to the effective FWHM laser pulse lengths of 2.21 ps (Fig. 4) and 0.902 ps (Fig. 5), respectively. Compared to the original laser pulse duration of 100 fs, the effective laser pulse length is dominated by the lengthening caused by oblique incidence. The beam charge was varied within the routine operation range of the UED

experiments, from 1 to 14 pC. The charge is measured by a Faraday Cup with an estimated accuracy of 0.1 pC. The minimum RMS bunch length of 1.8 ps was obtained with the laser spot size of 707 μm on the photocathode and the beam charge of 1 pC. The interferogram is shown in Figs. 4a. Figs. 4b and 4c show the corresponding interferograms for the beam charge of 2 pC and 14 pC, respectively. For the case with a laser spot size of 289 μm , the corresponding graphs are shown in Fig. 5 in the same order.

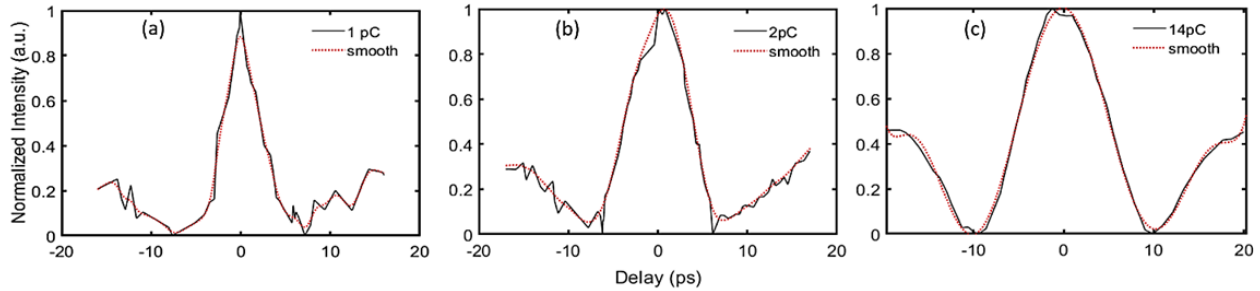


FIG. 4. In the case with a laser size of 707 μm on the photocathode, the measured field autocorrelation of sub-THz radiation for the charge 1pC (a), 2pC (b), and 14pC (c). In each plot, the dashed line represents the smoothed curve via moving average.

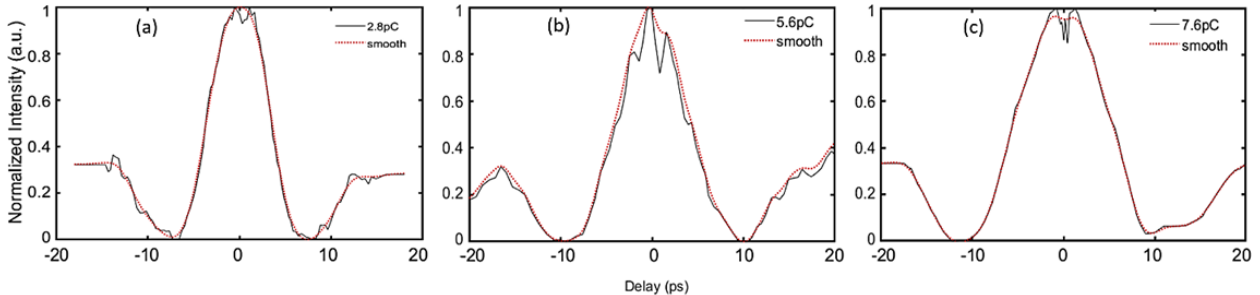


FIG. 5. In the case with a laser size of 289 μm , the measured field autocorrelation of sub-THz radiation for the charge 2.8 pC (a), 5.6 pC (b), and 7.6 pC (c). In each plot, the dashed line represents the smoothed curve via moving average.

3.2 Comparing Simulation with Experiment

Since the particle tracking code GPT takes the 3D space charge effect into account, and has been benchmarked with well-established simulation codes, such as ASTRA and PARMELA³²⁻³⁵, we consider a GPT model as a valid representation of the UED instrument. To build a model via the GPT code, we simulated two different configurations: 1) the beam charge of 14 pC at the effective laser pulse length of 0.942 ps (RMS) and 2) the beam charge of 7.6 pC at the effective laser pulse length of 0.385 ps (RMS). For both configurations, Fig. 6 shows the simulated bunch

lengths (red and black curves) in a reasonably good agreements with the measured bunch lengths (red square and black circle) at the position of the Al target (radiator), $z = 2.2 \text{ m}$ from the photocathode. Since the bunch length measurement can only be performed at the radiator position, the GPT model can be extremely useful for building a virtual diagnostic tool, which can make fast predictions of the electron bunch length³⁶ anywhere along the UED beamline. This tool can be useful for real-time optimization of the bunch length at the sample position to achieve high temporal resolution³⁷.

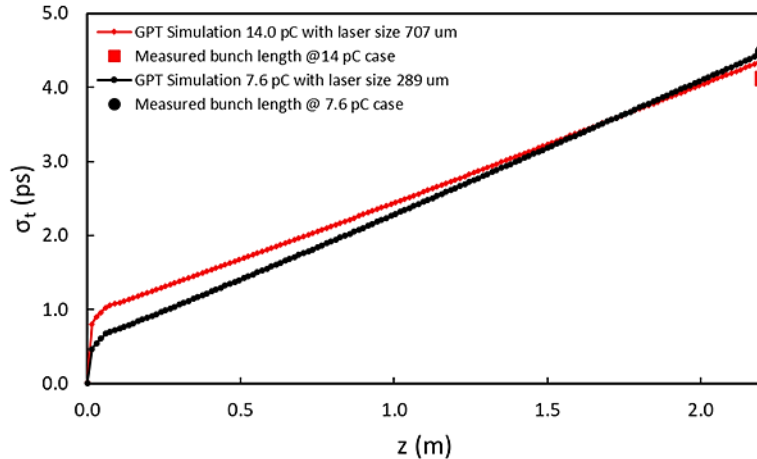


FIG. 6. Bunch lengths in the UED beamline at two different configurations: the charge of 14 pC (red) with the effective laser pulse length of 0.942 ps (RMS) and the charge of 7.6 pC (black) with the effective laser pulse length of 0.385 ps (RMS). The simulated bunch lengths (red and black curves) agree reasonably well with the measured bunch lengths at $z = 2.2 \text{ m}$ (red square and black circle), respectively.

Bunch length measurements consist of 4.3 ps for 14 pC and 4.5 ps for 7.6 pC. The bunch length of the low-energy electron beam is primarily dominated by the space charge effect. Increasing the laser spot size on the photocathode reduces the charge density and mitigates the space charge effects. Therefore, we observed smaller bunch lengthening in the case of 707 μm laser size and 14 pC charge compared to the case of 289 μm laser size and 7.6 pC charge. These results can be applied to calibrate the GPT model, building a virtual diagnostic tool of the longitudinal electron bunch profile monitor. Detailed studies of electron beam dynamics are beyond the scope of our paper.

Fig. 7a shows the measured bunch length as a function of the beam charge for two different laser sizes on the photocathode: the large size of 707 μm (black dots) and the small size of 289 μm

(red dots). The bunch lengths predicted by the GPT model are also plotted as cyan (large size) and green (small size) dots. Subtracting the effective bunch length at zero beam charge from all the data points in Fig. 7a provides the relative bunch lengthening $\Delta\sigma_t$, shown in Fig. 7b. Here, the effective bunch length at zero charge is estimated via Eq. (1), mainly due to the oblique incidence. The large and small laser sizes, 707 μm and 289 μm , contribute to the effective bunch lengths of 0.942 ps and 0.385 ps in RMS, respectively. Then, the zero-charge bunch length is estimated via convoluting the effective bunch length with the duration of the drive laser pulse, 0.1 ps in RMS; the results are 0.948 ps and 0.398 ps. A steeper dependency of the bunch lengthening with the charge appears in the small laser spot size case compared to the large laser spot size case, shown as the red (289 μm) and black (707 μm) dashed lines in Fig. 7b, respectively. According to the GPT simulation results shown in Fig. 6, the bunch lengthening with the charge could also depend on the longitudinal position where the measurement is performed; the calibrated GPT model can help us to understand this dependence.

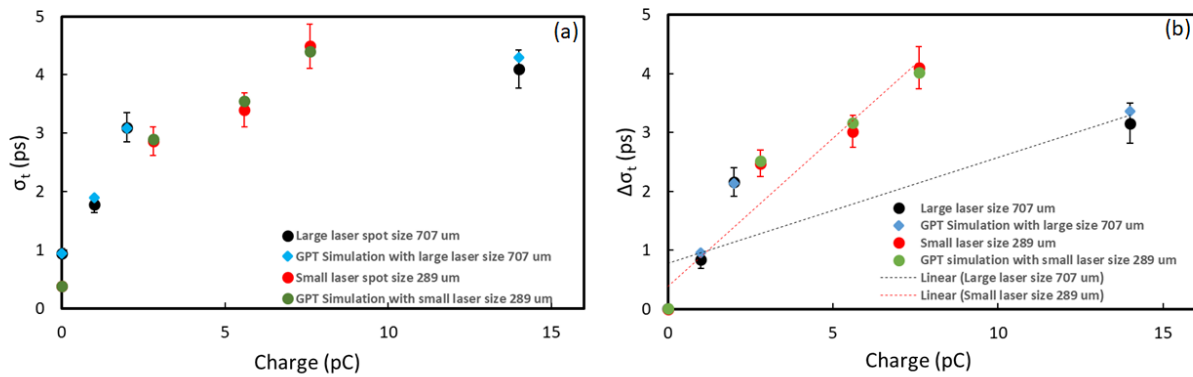


FIG. 7. (a) The measured RMS bunch lengths as a function of charge of the electron beam at two different laser sizes on the photocathode: 707 μm (black dots) and 289 μm (red dots). GPT simulation: cyan and green dots, respectively. The errors are estimated via the RMS deviation of three scans for each configuration. The contributing factors to the measurement errors are the shot-to-shot energy jitter, the laser intensity fluctuation, and the uncertainty of the delay τ . The errors at the zero-charge condition are inferred from the variation of the effective bunch length contributed by the measurement error of the laser-spot size on the photocathode. (b) For the same data set, the relative bunch lengthening $\Delta\sigma_t$ referring to the bunch length at zero charge are plotted with the similar colors. The black and red dashed lines represent the slope of bunch lengthening with charge at large (707 μm) and small (289 μm) sizes, respectively.

3.3 Discussion

Based on the experimental calibration using an electron beam with a charge of 10 pC and the bunch length of $\sigma_t = 4.0$ ps, the QOD signal at the peak of the interferogram was 500 mV. The combination of $\text{SNR} \geq 6$ and the noise level of 5 mV requires the minimum QOD signal of 30 mV. Fig. 8a helps to understand this: a calculated interferogram is shown as the red curve; a minimum of ten data points (blue circles) largely preserves the shape of the interferogram; the signals at two sides of the interferogram (light blue areas) should exceed the noise by at least a factor of two. As the result, the combination of $\text{SNR} \geq 6$ at the peak of the interferogram and the number of data points ≥ 10 can guarantee the high fidelity of the bunch length measurement.

In most cases, the maximum measurable bunch length is determined by the criteria that the QOD signal must be larger than 30 mV at the peak of the interferogram. The minimum measurable bunch length is limited by the step size of the movable mirror and the number of data points required to resolve the interferogram. The electron bunch profile is assumed to be Gaussian. The combination of the shortest bunch and lowest charge that can be measured by the QOD detector is determined by the condition where the maximum and minimum measurable bunch lengths merge, at the charge of 70 fC and the bunch length of 130 fs. The green area in Fig. 8b covers the region of the measurable bunch length depending on the charge. The combination of the shortest bunch and minimum charge is indicated by the red dot.

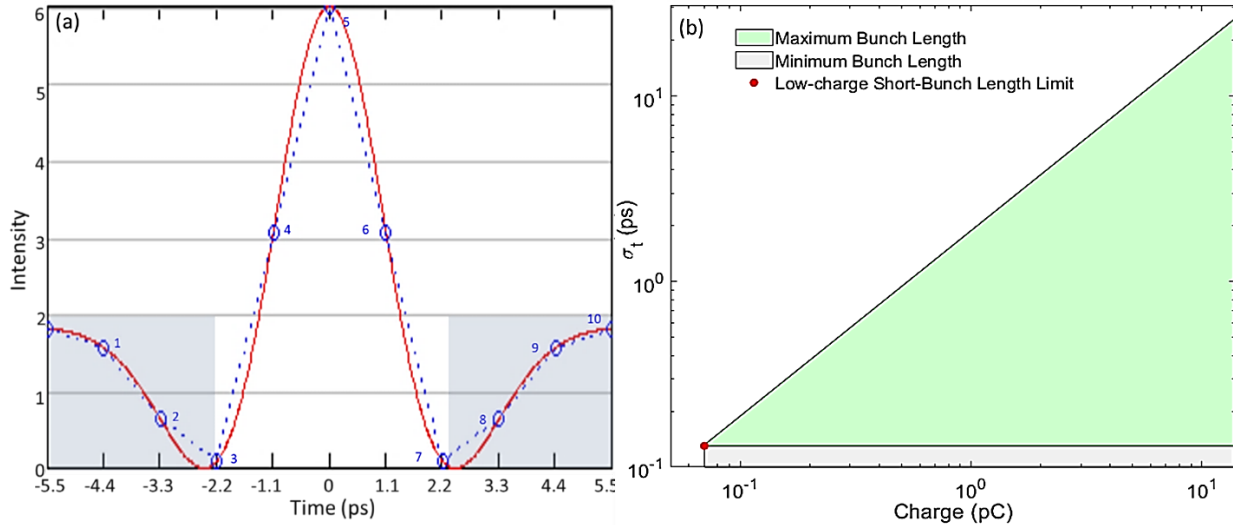


FIG. 8. (a) A calculated interferogram is shown as the red curve; limited ten data points covering the whole interferogram is shown as blue circles. The simulation is done with the RMS bunch length of 1 ps. (b) The measurable bunch length vs charge via the QOD detector is shown as the light green area. The limit of the

shortest bunch and minimum charge is shown as the red dot with the charge of 70 fC and the bunch length of 130 fs.

IV. CONCLUSION

We experimentally demonstrated the bunch length measurement of a 3 MeV electron beam with picocoulomb charge using the interferometric method. The use of a room-temperature QOD is critical for this measurement, given its SNR performance, proving to be more than 20 times higher in the sub-THz frequency range than that of a bolometer, in addition, eliminating the need for liquid-helium cooling, greatly simplified the experimental setup. In our experiment, the picosecond bunch length is only limited by the present photocathode drive laser setup and the distance from the cathode to the radiator. The advantages of using an interferometer compared to the technique based on ultrafast-laser-pump and electron-beam-probe include: the experimental setup is simple; no measurement error caused by the timing jitter between the laser and electron beams; the method can be easily extended to a broader range from sub- to tens- picosecond. In the future, we plan to build a virtual diagnostic tool based on the GPT model calibrated via the interferometric method.

Acknowledgements

This work is supported by the laboratory-directed research and development (LDRD) funding of BNL. The authors would like to thank Wayne Rambo, King Wilson, Christopher Danneil, Anthony Caracappa, Arturo Munoz, and Marcos Ruelas for technical supports, and Yuzhen Shen for many helpful discussions.

Data Availability

The data that support the findings of this study are available from the corresponding authors upon reasonable request.

References

1. L. Yu, Y. Zhu, T. Shaftan, L. Doom, BNL LDRD # 16-010, 63 (2016).
https://www.bnl.gov/lrd/files/pdf/2016_LDRD_Activities.pdf
2. Zhu, P., Y. Zhu, Y. Hidaka, L. Wu, J. Cao, H. Berger, J. Geck, R. Kraus, S. Pjerov, Y. Shen, R. Tobey, J.P. Hill, and X.J. Wang, "Femtosecond time-resolved MeV electron diffraction," *New J. of Physics* **17**, 063004 (2015).
3. A. He, F. Willeke, and L. H. Yu, "Ultrashort x-ray pulse generation by electron beam slicing in storage rings," *Phys. Rev. ST Accel. Beams* **17**, 040701 (2014).

4. A. He, F. Willeke, L. H. Yu, L. Yang, T. Shaftan, G. Wang, Y. Li, Y. Hidaka, and J. Qiang, "Design of low energy bunch compressors with space charge effects," *Phys. Rev. ST Accel. Beams* **18**, 014201 (2015).
5. H. N. Chapman, *et al.*, "Femtosecond diffractive imaging with a soft-X-ray free-electron laser," *Nat. Phys.* **2**, 839–843 (2006).
6. J. Yang, *et al.*, "Diffractive imaging of a rotational wavepacket in nitrogen molecules with femtosecond megaelectronvolt electron pulses," *Nat. Commun.* **05**, 11232 (2016).
7. J. Cao, X. Wang, and D. Zhong, "Mapping the structural dynamics of water dissociation", *Science* **374**, 34 (2021).
8. M.-F. Lin, N. Singh, S. Liang, M. Mo, J. P. F. Nunes, K. Ledbetter, J. Yang, M. Kozina, S. Weathersby, X. Shen, A. A. Cordones, T. J. A. Wolf, C. D. Pemmaraju, M. Ihme and X. J. Wang, "Imaging the short-lived hydroxyl-hydronium pair in ionized liquid water", *Science* **374**, 92 (2021).
9. X. Yang, *et al.*, "A compact tunable quadrupole lens for brighter and sharper ultra-fast electron diffraction imaging," *Sci. Rep.* **9**, 5115 (2019).
10. S. P. Weathersby, *et al.*, "Mega-electron-volt ultrafast electron diffraction at SLAC National Accelerator Laboratory," *Rev. Sci. Instrum.* **86**, 073702 (2015).
11. W. E. King, G. H. Campbell, A. Frank, B. Reed, J. F. Schmerge, B. J. Siwick, B. C. Stuart, and P. M. Weber, "Ultrafast electron microscopy in materials science, biology, and chemistry," *J. Appl. Phys.* **97**, 111101 (2005).
12. A. H. Zewail, "ULTRAFAST ELECTRON DIFFRACTION, CRYSTALLOGRAPHY, AND MICROSCOPY," *Annu. Rev. Phys. Chem.* **57**, 65 (2006).
13. G. Sciaini and R. J. D. Miller, "Femtosecond electron diffraction: heralding the era of atomically resolved dynamics," *Rep. Prog. Phys.* **74**, 096101 (2011).
14. P. Musumeci and R. K. Li, in ICFA Beam Dynamics Newsletter No. 59, edited by J. M. Byrd and W. Chou (International Committee for Future Accelerators, 2012), pp. 13–33.
15. X. Yang, *et al.*, "A novel nondestructive diagnostic method for mega-electron-volt ultrafast electron diffraction," *Sci. Rep.* **9**, 17223 (2019).
16. X. Yang, W. Wan, L. Wu, V. Smaluk, T. Shaftan, and Y. Zhu, "Toward monochromated sub-nanometer UEM and femtosecond UED," *Sci. Rep.* **10**, 16171 (2020).
17. Z. Zhang, X. Yang, X. Huang, J. Li, T. Shaftan, V. Smaluk, M. Song, W. Wan, L. Wu, and Y. Zhu, "Accurate prediction of mega- electron- volt electron beam properties from UED using machine learning," *Sci. Rep.* **11**, 13890 (2021).
18. M. De Loos and S. Van Der Geer, "General Particle Tracer: A new 3D code for accelerator and beamline design," 5th European Particle Accelerator Conference (EPAC, Barcelona, 1996), p. 1241
19. L. Zhao, *et al.*, "Terahertz Streaking of Few-Femtosecond Relativistic Electron Beams," *Phys. Rev. X* **8**, 021061 (2018).
20. L. Zhao, *et al.*, "Terahertz Oscilloscope for Recording Time Information of Ultrashort Electron Beams," *Phys. Rev. Lett.* **122**, 144801 (2019).
21. K. Sokolowski-Tinten, *et al.*, "Femtosecond X-ray measurement of coherent lattice vibrations near the Lindemann stability limit," *Nature* **422**, 287 (2003).
22. D. M. Fritz, *et al.*, "Ultrafast Bond Softening in Bismuth: Mapping a Solid's Interatomic Potential with X-rays," *Science* **315**, 633 (2007).
23. <https://acst.de/products/quasi-optical-detectors/>
24. Y. Shibata, *et al.*, "Observation of coherent transition radiation at millimeter and submillimeter wavelengths," *Phys. Rev. A* **45**, R8340 (1992).
25. http://www.tydexoptics.com/pdf/THz_Materials.pdf
26. H. C. Lihn, P. Kung, C. Settakorn, H. Wiedemann, and D. Bocek, "Measurement of subpicosecond electron pulses," *Phys. Rev. E* **53**, 6413 (1996).

27. K. Kan, M. Gohdo, T. Kondoh, I. Nozawa, J. Yang, Y. Yoshida, “MEASUREMENT OF FEMTOSECOND ELECTRON BEAM BASED ON FREQUENCY AND TIME DOMAIN SCHEMES,” Proceedings of IBIC 2016, Barcelona, Spain, pp. 483-485.
28. J. B. Rosenzweig, A. Murokh and A. Tremaine, “Coherent transition radiation-based diagnosis of electron beam pulse shape,” *AIP Conference Proceedings* **472**, 38 (1999)
29. U. Happek, A.J. Sievers and E.B. Blum, “Observation of coherent transition radiation,” *Phys. Rev. Lett.* **67**, 2962 (1991).
30. Y. Shen, X. Yang, G. L. Carr, Y. Hidaka, J. B. Murphy, and X. Wang, “Tunable Few-Cycle and Multicycle Coherent Terahertz Radiation from Relativistic Electrons,” *Phys. Rev. Lett.* **107**, 204801 (2011).
31. <https://www.irlabs.com/products/bolometers/>
32. Pulsar Physics and the General Particle Tracer (GPT) code, <http://www.pulsar.nl/index.htm>
33. I. Petrushina *et al.*, “High-Brightness Continuous-Wave Electron Beams from Superconducting Radio-Frequency Photoemission Gun,” *Phys. Rev. Lett.* **124**, 244801 (2020).
34. K. Flöttmann, “ASTRA: A Space Charge Tracking Algorithm,” DESY, Hamburg, Germany, 2000, <https://www.desy.de/~mpyflo/>
35. L. M. Young and J. H. Billen, Parmela, Los Alamos National Laboratory Report No. LA-UR-96-1835, 1996.
36. S. Nagaitsev, Z. Huang, J. Power, J.-L. Vay, P. Piot, L. Spentzouris, J. Rosenzweig, Y. Cai, S. Cousineau, and M. Conde *et al.*, “Accelerator and beam physics research goals and opportunities,” **arXiv:2101.04107**.
37. C. Emma, A. Edelen, M. J. Hogan, B. O’Shea, G. White, and V. Yakimenko, “Machine learning-based longitudinal phase space prediction of particle accelerators,” *Phys. Rev. Accel. Beams* **21**, 112802 (2018).